Available online at www.ijournalse.org

Emerging Science Journal

(ISSN: 2610-9182)

Vol. 9, No. 6, December, 2025

Rateless Polar Codes Exploiting Repetition Coding Principle with EXIT Analysis for Broadband Transmissions

Yuyun Siti Rohmah [1, 2], Iskandar [1], Khoirul Anwar [2], M. Sigit Arifianto [1*]

[1] *School of Electrical Engineering and Informatics Institut Teknologi Bandung, Jl. Ganesha No. 10, Bandung, Indonesia.*

[2] *The University Center of Excellence for Advanced Intelligent Communications (AICOMS), Telkom University, Bandung, Indonesia.*

Abstract

This paper proposes a novel design of polar codes for rateless transmissions employing extended parity (EP) to enhance performance under broadband channel conditions. The idea of the proposed design is to achieve diversity across all samples by employing simple butterfly XOR operations, which inherently support rateless broadband transmissions. In particular, the design exploits the principle of repetition, where simple XOR operations do not only contribute to error protection but also strengthen the polarization effect and reinforce the rateless property of polar codes. The proposed codes are evaluated over Rayleigh fading, fully interleaved, and additive white Gaussian noise (AWGN) channels. The results show that the proposed codes achieve significant performance improvements, particularly in AWGN and fully interleaved environments, thereby confirming that the use of XOR operations effectively enhances transmission reliability. Furthermore, the proposed codes are investigated through extrinsic information transfer (EXIT) analysis using closed-form expressions. The analysis reveals that the decoding process exhibits faster convergence when EP is employed. In addition, computational complexity analysis shows that the additional overhead introduced by EP remains minimal. Importantly, the proposed structure preserves the standard polar transform and decoding graph, ensuring scalability similar to conventional polar codes. Hence, the proposed design balances performance and computational efficiency, making it a compelling solution for broadband scenarios and dynamic channel environments.

Keywords:

Rateless;
Polar Codes;
Extended Parity;
Butterfly XOR Operations;
Broadband Transmission.

Article History:

Received:	04	August	2025
Revised:	12	October	2025
Accepted:	02	November	2025
Published:	01	December	2025

1- Introduction

The advent of sixth-generation (6G) networks introduces stringent requirements for channel coding to support diverse services such as ultra-reliable low latency communications (URLLC), massive machine-type communications (mMTC), and broadband immersive applications. Error control codes must deliver reliable performance under short block-length coding channels, adapt to dynamic channel variations, and minimize decoding latency for real-time services. At the same time, energy efficiency and low-complexity implementations are essential to prolong device lifetime in battery-constrained environments. Consequently, next-generation coding techniques must provide capacity-approaching performance while ensuring adaptability, scalability, and hardware-friendly designs, making them indispensable for future 6G communication systems [1].

In response to these requirements, several short block-length coding techniques have been explored in the literature. For example, the work in Yang et al. [2] presents distance spectrum optimal (DSO) convolutional codes aided by cyclic redundancy check (CRC), while Sui et al. [3] investigates high-rate convolutional codes enhanced by CRC and list

* **CONTACT**: arifianto@itb.ac.id

DOI: http://dx.doi.org/10.28991/ESJ-2025-09-06-020

decoding. In Ranganathan et al. [4], a quasi-cyclic protograph-based Raptor-like low-density parity-check (LDPC) design is proposed to meet stringent frame error rate (FER) targets at short lengths. These works highlight that short block-length coding is a practical necessity in 6G, enabling energy-efficient, low-latency, and reliable communication for services such as URLLC and mMTC.

Polar codes, introduced by Arıkan [5], have emerged as a promising candidate for short block-length transmission owing to their capacity-achieving performance under low-complexity successive cancellation (SC) decoding. Based on the principle of channel polarization, polar codes transform a set of identical channels into a mixture of highly reliable and unreliable sub-channels, where the butterfly computation unit plays a central role in enabling efficient encoding and decoding. Recent efforts to improve polar codes for short block-length regimes include the CRC-aided polar scheme under maximum likelihood (ML) decoding [6], the introduction of deep polar codes for improved block error rate [7], and hybrid multi-kernel constructions tailored for energy-constrained devices [8]. Further advances include low-latency polar decoders with parallelism-aware subtree pruning [9], and the integration of polar-coded modulation into relay systems operating at short lengths [10]. Nevertheless, despite these significant advancements in reliability, decoding efficiency, and structural design, the existing approaches were not conceived for rateless transmission and therefore cannot dynamically adjust redundancy to accommodate time-varying channel conditions, which remains an open challenge for adaptive coding in 6G systems.

Random variations in channel conditions result in fluctuating channel capacity C, which degrades the quality of the received signal. Fixed-rate coding schemes inherently limit the system's ability to adapt to such rapid channel dynamics. When fixed-rate coding is used, scenarios may arise where C decreases below the coding rate R, making reliable communication infeasible. According to Shannon's theorem, effective communication is possible only if $R \leq C$. By employing rateless channel coding, the coding rate is dynamically adjusted to remain within the channel capacity, ensuring reliable transmission.

To overcome the limitations of fixed-rate coding, rateless coding schemes dynamically adjust the coding rate R in response to channel variations. LT codes, introduced in Luby [11], represent the first practical realization of rateless codes, employing receiver feedback to adapt the degree distribution and maintain rate compatibility. However, in additive white Gaussian noise (AWGN) and fading channels, LT codes suffer from an error floor due to suboptimal degree distributions and the absence of soft-decision decoding. To mitigate these issues, enhancements such as accumulator-aided encoding [12] and Tornado-based architectures [13] have been proposed. Beyond these improvements, other approaches include Raptor codes tailored for low-power biomedical telemetry [14] and Reed–Solomon-based rateless codes offering zero overhead for short block-lengths [15].

Beyond conventional rateless designs, polar codes have emerged as a promising alternative for achieving rateless transmission. Several schemes have been proposed in the literature. In Liang et al. [16], a novel rateless scheme is proposed by extending and puncturing polar codes for unknown AWGN channels. Similarly, rateless polar codes based on puncturing are further investigated in Schnelling et al. [17]. In Liang et al. [18], a rateless coding scheme with improved unequal error protection (UEP) is introduced by combining systematic polar codes (SPC) as the outer code and Spinal codes as the inner code. Another scheme is presented in Feng et al. [19], where a rateless design leverages the extendibility of systematic polar codes to address scenarios with unavailable CSI. Further developments include the IF-RC and EC-RC schemes proposed in Li et al. [20] and Liang et al. [21] which enable smooth rate adaptation under unpredictable channel conditions. However, these studies primarily focus on rateless design for AWGN or generic fading channels and do not address the specific challenges of broadband transmissions, such as frequency selectivity and rich diversity inherent in wideband environments.

Broadband channels with frequency-selective fading and diversity-rich environments, such as multipath propagation or block fading, impose stringent requirements on coding schemes. Reliable transmission in such conditions demands coding strategies capable of exploiting channel diversity while adapting to rapid channel fluctuations. In Liu et al. [22], polar codes were extended to block fading channels by aligning code construction with fading polarization, which enabled efficient exploitation of diversity. In Niu & Li [23], the polar spectrum framework was proposed to design full-diversity polar codes, further improving error performance while preserving low complexity.

Existing schemes remain limited in simultaneously achieving rateless adaptability, broadband diversity, and reliable performance at short block-lengths. Most prior studies either focus on rate adaptation in AWGN and generic fading channels, or exploit diversity in block-fading scenarios without incorporating the inherent flexibility of rateless coding. These limitations highlight the design of rateless polar codes tailored for broadband transmissions, where extended parity mechanisms can be employed to ensure diversity across all samples, support short block-length operation, and preserve low complexity.

Motivated by these advancements, this paper proposes a novel rateless polar coding scheme employing extended parity (EP) to improve adaptability and robustness in broadband channel conditions, while incurring only minimal computational overhead. The terminology that aligns with the common understanding is the extended parity-check,

however, for simplicity, we use the term of the extended parity. A series of computer simulations is conducted to evaluate the performance of the proposed codes in terms of average bit error rate (BER) and average frame error rate (FER) over Rayleigh fading, fully interleaved, and additive white Gaussian noise (AWGN) channels. To validate the performance of the proposed structure, we utilize the extrinsic information transfer (EXIT) chart analysis introduced in Brink and Ten [24] and derive a closed-form expression for the elementary extrinsic mutual information. Furthermore, we express the proposed codes similarly to LDPC codes, as introduced in Gallager [25] using Tanner graphs, the generator matrix **G** and the parity check matrix **H**. Finally, we analyze the computational complexity of the proposed design. The contributions of this paper are summarized as follows:

- A novel rateless coding structure based on polar codes for broadband channels: This paper proposes a novel rateless coding structure based on Arıkan polar codes combined with butterfly XOR operations-based extended parity (EP) under broadband channel [*].
- EXIT chart analysis: The performance of the proposed codes evaluated through an EXIT chart analysis. We present the elementary EXIT curves and derive a closed-form expression for the extrinsic mutual information.

The rest of this paper is organized as follows. Section II describes the system model. Section III presents the design of the proposed codes, including the encoder, decoder, and their rate adaptability. This section also includes the EXIT chart analysis of the proposed codes and introduces their representation using Tanner graphs and corresponding matrices, similar to LDPC codes. Section IV evaluates the performance of the proposed codes design through numerical simulations, providing a detailed analysis of the bit error rate (BER), frame error rate (FER), and complexity. Finally, Section V concludes the paper.

2- System Model

In this paper, we propose a novel design of polar codes for rateless transmission using EP to enhance broadband channel. The proposed design utilizes Arıkan's polar codes as the mother code (MC) and butterfly XOR operations to generate the EP. The inclusion of EP bits results in a proportional increase in butterfly XOR operations, with each additional EP bit requiring one corresponding butterfly XOR operation. The rateless transmission mechanism is implemented by progressively adding parity bits, starting from one and increasing to two or more, as required. The number of EP bits is dynamically adjusted according to R, which is adaptively matched to instantaneous C.

The system model of the proposed codes with the EP, illustrated for a block-length of $N = 16$ and $R = 4/16$ is shown in Figure 1. The proposed structure is scalable to larger values of N. As illustrated in Figure 1, a set of $k = 4$ binary information bits, denoted as $\mathbf{b} = [b_1, b_2, b_3, b_4]$, is generated and fed into the encoding block of $= [u_1, u_2, u_3, u_5]$, respectively. The remaining bits, $[u_4, u_6, u_7, u_8]$, are assigned as frozen bits, while $[u_9, \cdots, u_{16}]$ represent EP bits. In this structure, the proposed codes support a variable coding rate, given by $R = \{4/8, 4/9, \ldots, 4/16\}$. The EP bits are initialized to zero similar with frozen bits. The proposed codes then generate the codewords $\mathbf{c} = [c_1, c_2, \cdots, c_{16}]$, which are subsequently mapped to binary modulated symbols **x** using binary phase shift keying (BPSK). These symbols are then transmitted over a channel characterized by h.

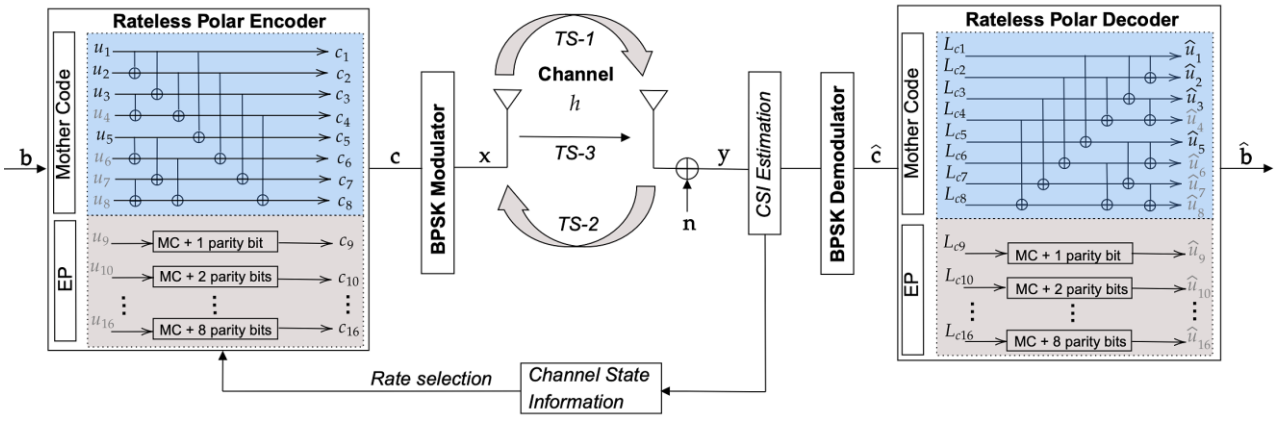

Figure 1. The system model of the proposed codes using the EP with $R = 4/16$ and $N = 16$

The channel is assumed to remain constant over three consecutive time slots, denoted as TS-1, TS-2, and TS-3. In TS-1, the transmitter (Tx) initiates the transmission using a fixed coding rate. In TS-2, the receiver (Rx) performs channel estimation based on observed signal-to-noise ratio (SNR) and fading condition. The estimated channel state information

[*] The proposed design may exhibit inferior performance compared to conventional coding techniques such as repetition codes in the short block-length regime, this limitation is expected to diminish as the block-length increases since the quality of polarization is increasing in large block-length. However, performance analysis for large block-lengths is beyond the scope of this paper. As such, this study serves as an initial investigation into the feasibility of constructing polar codes for rateless transmission.

(CSI) is then fed back to the transmitter through an ideal, noise-free feedback link. In TS-3, the transmitter adjusts R by appending an appropriate number of EP bits such that the overall redundancy aligns with the estimated. This adaptive transmission strategy enhances spectral efficiency while reducing unnecessary retransmissions. Once the system enters TS-4, the channel may vary, thereby invalidating the previously acquired CSI. A new estimation and feedback cycle is thus required to maintain the effectiveness of rate adaptation under changing channel conditions. In this paper, we assume that the CSI is perfectly known at the transmitter. Consequently, the sensitivity of system performance to imperfect CSI estimation is beyond the scope of this paper and is left as an interesting direction for future research.

Since this paper considers a point-to-point communication system, the complexity of equalization is omitted for simplicity. The received signal is expressed as:

$$\mathbf{y} = h\mathbf{x} + \mathbf{n}\,, \tag{1}$$

where $\mathbf{y}$ denotes the received signal, h is the channel coefficient, and $\mathbf{n}$ represents the additive white Gaussian noise (AWGN) with zero mean and variance σ^2. At the receiver, $\mathbf{y}$ is demodulated to produce log-likelihood ratio (LLR) values, denoted as $\hat{\mathbf{c}}$. These values, represented as $L_c = [L_{c1}, L_{c2}, \cdots, L_{c16}]$, are decoded using the successive-cancellation (SC) algorithm, which iteratively processes the received sequence to estimate the transmitted information. The resulting vector $\hat{\mathbf{b}}$, expressed as $\hat{\mathbf{u}} = [\hat{u}_1, \hat{u}_2, \hat{u}_3, \hat{u}_5]$, represents the estimated information bits and is used to evaluate the performance of the proposed codes under all channels.

3- The Proposed Rateless Polar Codes for Broadband Transmissions

Three key requirements are established for designing the proposed structure. First, following Arıkan's principle of polarization in polar codes, the capacity gap between the highest and lowest values must be sufficiently large to ensure effective polarization. Second, the decoding process must achieve high accuracy to maintain reliable communication. Third, the coding structure must demonstrate adaptability to variations in channel capacity, thereby facilitating the implementation of a rateless coding design.

3-1- Encoder Structure

Figure 2 illustrates an example of the encoder structure of the proposed codes with $R = 4/16$ and $N = 16$. The encoder structure consists of two primary components: the MC and the EP blocks. The EP is constructed from the MC with $R = 4/8$. The rateless transmission mechanism is enabled by incrementally adding one or more EP bits to the MC in order to adapt to variations in channel capacity. This example supports rate adaptability within the range of $R = 4/8$ to $R = 4/16$, with the potential for extension to a wider range of R for larger values of N. Figure 3 presents an example of the encoder for the proposed codes with $N = 32$ and $R = 8/32$, where MC operates with $R = 8/16$. The proposed structure preserves the standard polar transform and decoding graph, and therefore it can be scaled in the same manner as Arıkan's original polar codes.

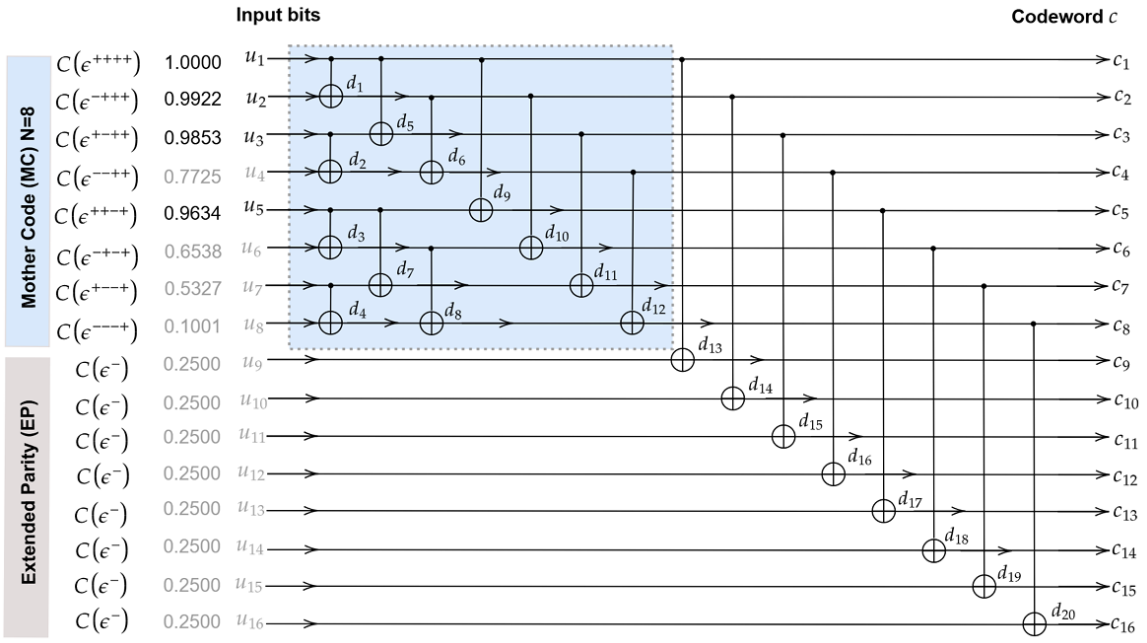

Figure 2. Example of the encoder structure of the proposed codes with $= 4/16$, where EP is constructed from a MC with $R = 4/8$

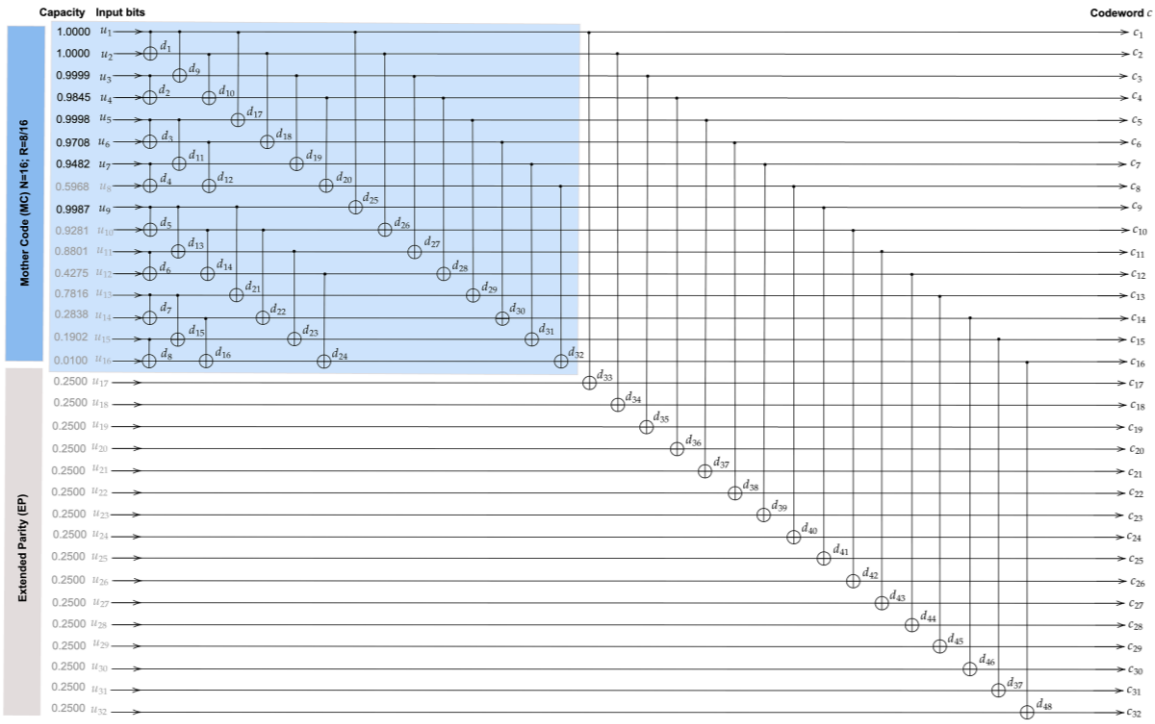

Figure 3. Example of the encoder structure of the proposed codes with $R = 8/32$, where EP is constructed from a MC with $R = 8/16$

The EP structure of the proposed codes adopts a staircase-like configuration, where butterfly units are integrated sequentially and interdependently. The inclusion of each EP bit requires one butterfly unit, resulting in linear scalability when multiple EP bits are added. A simplified EP structure is designed to maximize the capacity gap between the strongest and weakest polarized subchannels within the MC and EP blocks. This design ensures that elements designated as EP do not attain high capacity, thereby preserving the polarization principle of the coding structure.

In this paper, the selection of information and frozen bit positions in the proposed structure is based on subchannel capacity estimation of the polarization channel, as introduced by Arıkan using the binary erasure channel (BEC) model. Although the proposed scheme is evaluated over Rayleigh fading, fully interleaved, and AWGN channels, the BEC capacity $C(W)$ is adopted as a surrogate metric for bit-channel reliability. This choice is motivated by the seminal work of Arıkan, where the BEC model was used to derive Bhattacharyya parameters $Z(W)$ that characterize the polarization behavior of bit-channels in polar codes. Despite its simplicity, the BEC-based reliability sequence has been shown to provide near-optimal performance.

The channel capacity of BEC is defined as $C(W) = 1 - \epsilon$, where ϵ represents the erasure probability, and is bounded by $0 \leq C(W) \leq 1$. The $Z(W)$ quantifies the reliability of a bit-channel, where a smaller value indicates higher reliability, constrained by $0 \leq \mathrm{Z(W)} \leq 1$. The Bhattacharyya parameter is expressed as $Z(W) = \epsilon$ for a BEC. If channel W is a BEC, the modified erasure probabilities ϵ^- and ϵ^+, are also characterized as BECs, with the corresponding erasure probabilities given by $\epsilon^- \triangleq 2\epsilon - \epsilon^2$ and $\epsilon^+ \triangleq \epsilon^2$, respectively.

Based on Figure 2, the capacity of each modified erasure channel in the proposed structure is evaluated using the Bhattacharyya parameter. For an erasure probability of $\epsilon = 0.5$, the channel capacities, in sequential order, are: 1.0000, 0.9922, 0.9853, 0.7725, 0.9634, 0.6538, 0.5327, 0.1001, 0.2500, 0.2500, 0.2500, 0.2500, 0.2500, 0.2500, 0.2500, and 0.2500. Among these, the $k = 4$ information bits are allocated to the first, second, third, and fifth subchannels. The remaining channels are designated for frozen bits, while the EP bits are assigned to the ninth through the last subchannels, with all EP bits set to 0. The encoding process of the proposed structure is based on a sequence of XOR operations, where each output d_i represents the result of the ith XOR computation. The sequence $d_i = [d_1, d_2, \cdots, d_{20}]$, reflects the total number of XOR operations performed during encoding and is subsequently used to construct the final codeword $\mathbf{c} = [c_1, c_2, \cdots, c_{16}]$. The codeword elements from c_1 to c_8 are computed as follows:

$$c_1 = u_1, \tag{2}$$

$$c_2 = u_1 \oplus u_2, \tag{3}$$

$$c_3 = u_1 \oplus u_3, \tag{4}$$

$$c_4 = u_1 \oplus u_2 \oplus u_3 \oplus u_4, \tag{5}$$

$$c_5 = u_1 \oplus u_5, \tag{6}$$

$$c_6 = u_1 \oplus u_2 \oplus u_5 \oplus u_6, \quad (7)$$

$$c_7 = u_1 \oplus u_3 \oplus u_5 \oplus u_{7,} \quad (8)$$

$$c_8 = u_1 \oplus u_2 \oplus u_3 \oplus u_4 \oplus u_5 \oplus u_6 \oplus u_7 \oplus u_8. \quad (9)$$

Similarly, the codeword elements from c_9 to c_{16} are computed as follows:

$$c_9 = u_1 \oplus u_9, \quad (10)$$

$$c_{10} = u_1 \oplus u_2 \oplus u_{10}, \quad (11)$$

$$c_{11} = u_1 \oplus u_3 \oplus u_{11}, \quad (12)$$

$$c_{12} = u_1 \oplus u_2 \oplus u_3 \oplus u_4 \oplus u_{12}, \quad (13)$$

$$c_{13} = u_1 \oplus u_5 \oplus u_{13}, \quad (14)$$

$$c_{14} = u_1 \oplus u_2 \oplus u_5 \oplus u_6 \oplus u_{14}, \quad (15)$$

$$c_{15} = u_1 \oplus u_3 \oplus u_5 \oplus u_7 \oplus u_{15}, \quad (16)$$

$$c_{16} = u_1 \oplus u_2 \oplus u_3 \oplus u_4 \oplus u_5 \oplus u_6 \oplus u_7 \oplus u_8 \oplus u_{16}. \quad (17)$$

3-2- Decoder Structure

The decoding structure corresponding to the encoder in Figure 2 is illustrated in Figure 4 and employs the successive cancellation (SC) algorithm. The process involves computing log-likelihood ratio (LLR) values, L_1 through L_{32} along with L_A, L_B, L_C, and L_E, derived from the soft demapper output L_{cj} with $j = 1, 2, \cdots, 16$. These values are subsequently processed to estimate the information bits $\hat{\mathbf{u}} = [\hat{u}_1, \hat{u}_2, \hat{u}_3, \hat{u}_5]$. The decoding framework incorporates two primary operations: the box-plus and sum operations.

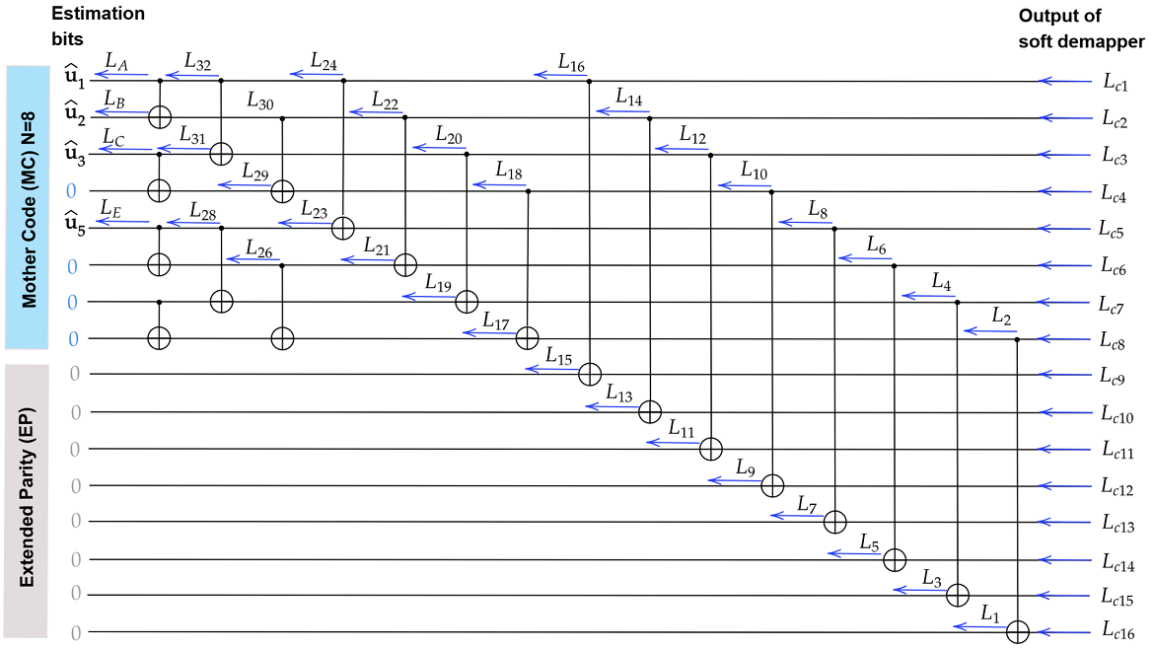

Figure 4. Example of the decoder structure of the proposed codes having $R = 4/16$

The box-plus operation, used to compute L_B is defined as $L_B \approx \left(sign(L_{30}) * sign(L_{32})\right) * min(|L_{30}|, |L_{32}|)$. Conversely, the sum operation is employed to calculate L_A, L_C, and L_E, given by $L_A = ((-1)^{\hat{u}_2} * L_{30}) + L_{32}$, $L_C = ((-1)^0 * L_{29}) + L_{31}$, $L_E = ((-1)^0 * L_{26}) + L_{28}$, respectively. In addition, the box-plus operation is systematically applied to $L_1, L_3, \cdots, L_{31}$, while the sum operation is utilized for $L_2, L_4, \cdots, L_{32}$. This hierarchical computation design enables efficient LLR processing, facilitating accurate bit estimation.

3-3- Rate Adaptability of The Proposed Codes

As described in Table 1, the rate adaptation mechanism for rateless transmission, corresponding to the encoder and decoder structures shown in Figures 2 and 4, respectively, dynamically adjusts R base on the estimated C. This approach aims to achieve an optimal trade-off between spectral efficiency and reliability under varying channel conditions. The mechanism modifies the number of EP bits to ensure that the condition $R \leq C$ is satisfied.

Table 1. The rate adaptation mechanism for the transition from $R = 4/8$ to $R = 4/16$

Conditions	Capacity (C)	Adopted Rate (R)
1	$C \geq 4/8$	$4/8$
2	$4/9 \leq C < 4/8$	$4/9$
3	$4/10 \leq C < 4/9$	$4/10$
4	$4/11 \leq C < 4/10$	$4/11$
5	$4/12 \leq C < 4/11$	$4/12$
6	$4/13 \leq C < 4/12$	$4/13$
7	$4/14 \leq C < 4/13$	$4/14$
8	$4/15 \leq C < 4/14$	$4/15$
9	$C < 4/15$	$4/16$

The transmitter is assumed to acquire perfect CSI via noise-free feedback from the receiver, which performs accurate channel estimation. This feedback enables the estimation of the channel capacity and informs decisions regarding the decision on the appropriate number of EP bits to be appended to MC. By varying the number of EP bits, R is adaptively adjusted to align with the evolving channel conditions.

As shown in Table 1, the proposed codes support nine distinct coding rates. These rates range from $R = 4/8$ to $R = 4/16$. For instance, when the channel capacity satisfies $4/9 \leq C < 4/8$, the system selects $R = 4/9$. This rate adaptation mechanism provides an effective strategy for addressing dynamic channel conditions in rateless transmission systems. The system ensures robust performance across a wide range of scenarios by selecting the optimal coding rate based on feedback from the receiver. Under high-capacity conditions $C \geq 4/8$, the system operates at a higher R, maximizing spectral efficiency while maintaining reliability. Conversely, as C decreases, the system progressively transitions to lower coding rates $R = \{4/9, \cdots, 4/16\}$, thereby increasing redundancy and enhancing error correction capabilities to accommodate more challenging channel conditions.

3-4- EXIT Chart Analysis of the Proposed Codes

An extrinsic information transfer (EXIT) chart is an analytical tool to evaluate the behavior of iterative decoding processes. It enables the prediction of decoding performance, such as the occurrence of error-floors and the required number of iterations without relying on extensive computer simulations. In this paper, the EXIT curves are analyzed to evaluate the decoding performance of the proposed design. The decoder structure, which incorporates the extrinsic mutual information I_E, and is derived from the decoder structure in Figure 4, is illustrated in Figure 5. Note that the EXIT analysis in this paper differs from the general EXIT approach, as polar codes are decoded element-wise under successive cancellation (SC). We therefore adopt the term elementary EXIT chart to evaluate the structure of the proposed codes. This analysis demonstrates the reliability of individual bit-channels, where the inclusion of EP bits accelerates the convergence of extrinsic mutual information curves and validates the placement of information and frozen bits. Consequently, the analysis primarily characterizes the waterfall region through its convergence properties, while the error floor is not explicitly predicted.

The elementary curves corresponding to the first, second, third, and fifth bit-channels, denoted as I_{E_1}, I_{E_2}, I_{E_3}, and I_{E_5}, are used to characterize bit-channel quality. The evaluation criterion is that all I_E curves converge at the point (1,1). Unlike EXIT charts by Brink, which compare inner/outer decoder transfer functions via a tunnel criterion, the proposed elementary EXIT charts report I_E (I_A) for each polarized bit-channel under SC decoding, thereby assessing bit-level reliability rather than inter-decoder matching.

The EXIT analysis for check nodes and variable nodes follows the same principles as those used in low-density parity-check (LDPC) codes, as described in Ten Brink et al. [26]. As illustrated in Figure 5, the computation of I_{E_1} is performed by considering the values of the priori information I_A with a fixed value of 1 for the frozen bits and EP bits, since their values are deterministically known unchanged. The same principle is applied to derive the values of I_{E_2}, I_{E_3}, and I_{E_5}. A related EXIT chart analysis for polar codes was presented in Mufassa & Anwar [27] , which provides insight into the channel transformation process.

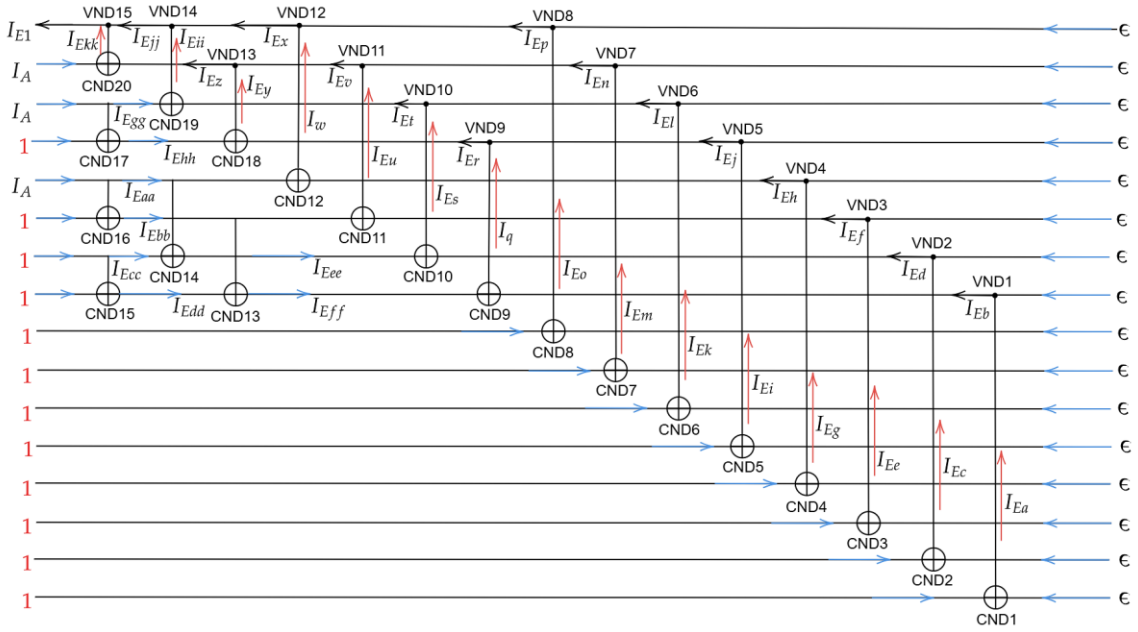

Figure 5. Decoder structure with mutual information notation used to draw the EXIT curve for the proposed codes with $R = 4/16$

According to Ten Brink et al. [26] , two operations are employed to derive the I_E : the variable node decoder (VND) and check node decoder (CND) operations. These operations are mathematically expressed as $I_{E,VND} = 1 - \epsilon \cdot \lambda(1 - I_{A,VND})$ and $I_{E,CND} = \omega(I_{A,CND})$, respectively, where $\lambda(\cdot)$ and $\omega(\cdot)$ represent the degree distributions of the VND and CND. As shown in Figure 5, the extrinsic mutual information values I_{Ea} and I_{Eb} are obtained through the CND and VND operations, respectively, and all subsequent I_E values are computed until I_{E_1}, I_{E_2}, I_{E_3}, and I_{E_5} are derived.

Based on the decoder structure depicted in Figure 5, the elementary mutual information I_{E_1}, I_{E_2}, I_{E_3}, and I_{E_5} for the proposed rateless polar codes are derived as follows:

$$I_{E_1} = -I_A{}^7\epsilon^{16} + 4I_A{}^7\epsilon^{14} - 6I_A{}^7\epsilon^{12} + 4I_A{}^7\epsilon^{10} - I_A{}^7\epsilon^8 - 4I_A{}^6\epsilon^{14} + 14I_A{}^6\epsilon^{12} - 18I_A{}^6\epsilon^{10} + 10I_A{}^6\epsilon^8 - 2I_A{}^6\epsilon^6 - 8I_A{}^5\epsilon^{12} + 24I_A{}^5\epsilon^8 + 10I_A{}^5\epsilon^6 - I_A{}^5\epsilon^4 - 10I_A{}^4\epsilon^{10} + 25I_A{}^4\epsilon^8 - 20I_A{}^4\epsilon^6 + 5I_A{}^4\epsilon^4 - 9I_A{}^3\epsilon^8 + 18I_A{}^3\epsilon^6 - 10I_A{}^3\epsilon^4 + I_A{}^3\epsilon^2 - 6I_A{}^2\epsilon^6 + 9I_A{}^2\epsilon^4 - 3I_A{}^2\epsilon^2 - 3I_A\epsilon^4 + 3I_A\epsilon^2 - \epsilon^2 + 1\,, \quad (18)$$

$$I_{E_2} = I_A{}^6\epsilon^{16} - 4I_A{}^6\epsilon^{14} + 6I_A{}^6\epsilon^{12} - 4I_A{}^6\epsilon^{10} + I_A{}^6\epsilon^8 + 4I_A{}^5\epsilon^{14} - 14I_A{}^5\epsilon^{12} + 18I_A{}^5\epsilon^{10} - 10I_A{}^5\epsilon^8 + 2I_A{}^5\epsilon^6 + 8I_A{}^4\epsilon^{12} - 24I_A{}^4\epsilon^{10} + 25I_A{}^4\epsilon^8 - 10I_A{}^4\epsilon^6 + I_A{}^4\epsilon^4 + 10I_A{}^3\epsilon^{10} - 26I_A{}^3\epsilon^8 + 22I_A{}^3\epsilon^6 - 6I_A{}^3\epsilon^4 + 8I_A{}^2\epsilon^8 + 18I_A{}^2\epsilon^6 + 12I_A{}^2\epsilon^4 - 2I_A{}^2\epsilon^2 + 4I_A\epsilon^6 - 8I_A\epsilon^4 + 4I_A\epsilon^2 + \epsilon^4 - 2\epsilon^2 + 1, \quad (19)$$

$$I_{E_3} = -I_A{}^4\epsilon^{16} + 4I_A{}^4\epsilon^{14} - 6I_A{}^4\epsilon^{12} + 4I_A{}^4\epsilon^{10} - I_A{}^4\epsilon^8 - 4I_A{}^3\epsilon^{14} + 16I_A{}^3\epsilon^{12} - 24I_A{}^3\epsilon^{10} + 16I_A{}^3\epsilon^8 - 4I_A{}^3\epsilon^6 - 6I_A{}^2\epsilon^{12} + 24I_A{}^2\epsilon^{10} - 34I_A{}^2\epsilon^8 + 20I_A{}^2\epsilon^6 - 4I_A{}^2\epsilon^4 - 4I_A\epsilon^{10} + 16I_A\epsilon^8 - 20I_A\epsilon^6 + 8I_A\epsilon^4 - \epsilon^8 + 4\epsilon^6 - 4\epsilon^4 + 1\,, \quad (20)$$

$$I_{E_5} = 1 - 16\epsilon^8 + 32\epsilon^{10} - 24\epsilon^{12} + 8\epsilon^{14} - \epsilon^{16}. \quad (21)$$

Therefore, as a benchmark, the elementary EXIT curves of the MC are also analyzed. Based on VND and CND operations, the extrinsic mutual information values I_{E_1}, I_{E_2}, I_{E_3}, and I_{E_5} for the MC are expressed as follows:

$$I_{E_1} = -I_A{}^7\epsilon^8 + 4I_A{}^7\epsilon^7 - 6I_A{}^7\epsilon^6 + 4I_A{}^7\epsilon^5 - I_A{}^7\epsilon^4 - 4I_A{}^6\epsilon^7 + 14I_A{}^6\epsilon^6 - 18I_A{}^6\epsilon^5 + 10I_A{}^6\epsilon^4 - 2I_A{}^6\epsilon^3 - 8I_A{}^5\epsilon^6 + 24I_A{}^5\epsilon^5 - 25I_A{}^5\epsilon^4 + 10I_A{}^5\epsilon^3 - I_A{}^5\epsilon^2 - 10I_A{}^4\epsilon^5 + 25I_A{}^4\epsilon^4 - 20I_A{}^4\epsilon^3 + 5I_A{}^4\epsilon^2 - 9I_A{}^3\epsilon^4 + 18I_A{}^3\epsilon^3 - 10I_A{}^3\epsilon^2 + I_A{}^3\epsilon - 6I_A{}^2\epsilon^3 + 9I_A{}^2\epsilon^2 - 3I_A{}^2\epsilon - 3I_A\epsilon^2 + 3I_A\epsilon - \epsilon + 1, \quad (22)$$

$$I_{E_2} = I_A{}^6\epsilon^8 - 4I_A{}^6\epsilon^7 + 6I_A{}^6\epsilon^6 - 4I_A{}^6\epsilon^5 + I_A{}^6\epsilon^4 + 4I_A{}^5\epsilon^7 - 14I_A{}^5\epsilon^6 + 18I_A{}^5\epsilon^5 - 10I_A{}^5\epsilon^4 + 2I_A{}^5\epsilon^3 + 8I_A{}^4\epsilon^6 - 24I_A{}^4\epsilon^5 + 25I_A{}^4\epsilon^4 - 10^4\epsilon^3 + I_A{}^4\epsilon^2 + 10I_A{}^3\epsilon^5 - 26I_A{}^3\epsilon^4 + 22I_A{}^3\epsilon^3 - 6I_A{}^3\epsilon^2 + 8I_A{}^2\epsilon^4 - 18I_A{}^2\epsilon^3 + 12I_A{}^2\epsilon^2 - 2I_A{}^2\epsilon + 4I_A\epsilon^3 - 8I_A\epsilon^2 + 4I_A\epsilon + \epsilon^2 - 2\epsilon + 1, \quad (23)$$

$$I_{E_3} = -I_A{}^4\epsilon^8 + 4I_A{}^4\epsilon^7 - 6I_A{}^4\epsilon^6 + 4I_A{}^4\epsilon^5 - I_A{}^4\epsilon^4 - 4I_A{}^3\epsilon^7 + 16I_A{}^3\epsilon^6 - 24I_A{}^3\epsilon^5 + 16I_A{}^3\epsilon^4 - 4I_A{}^3\epsilon^3 - 6I_A{}^2\epsilon^6 + 24I_A{}^2\epsilon^5 - 34I_A{}^2\epsilon^4 + 20I_A{}^2\epsilon^3 - 4I_A{}^2\epsilon^2 - 4I_A\epsilon^5 + 16I_A\epsilon^4 - 20I_A\epsilon^3 + 8I_A\epsilon^2 - \epsilon^4 + 4\epsilon^4 - 4\epsilon^2 + 1, \quad (24)$$

$$I_{E_5} = 1 - 16\epsilon^4 + 32\epsilon^5 - 24\epsilon^6 + 8\epsilon^7 - \epsilon^8. \quad (25)$$

Figure 6. illustrates the elementary EXIT curves I_{E_1}, I_{E_2}, I_{E_3}, and I_{E_5} for the proposed rateless polar codes, both without and with EP, under an erasure probability of $\epsilon = 0.75$. These curves represent the evolution of the extrinsic mutual information I_E as a function of the a priori information I_A. The analysis is based on BEC model, where the

subchannel capacity $C = 1 - \epsilon = 0.25$ serves as a theoretical benchmark for each bit-channel in the polarization process. This capacity is distinct from the overall channel capacity of the medium, which refers to the actual physical channel (AWGN or Rayleigh fading channels).

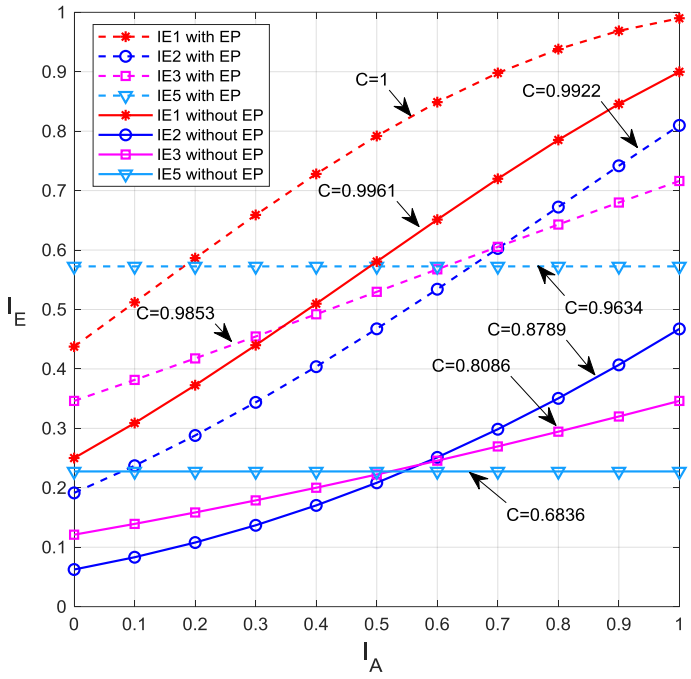

Figure 6. Elementary EXIT curves I_{E_1}, I_{E_2}, I_{E_3}, and I_{E_5} of the proposed codes without EP and with EP for $\epsilon = 0.75$

The results show that I_E curves with EP remain above the subchannel capacity threshold of 0.25 throughout the decoding process, indicating improved mutual information exchange. Among these, I_{E_1} exhibits the highest mutual information and achieves faster convergence than the other curves. Conversely, I_{E_2}, I_{E_3}, and I_{E_5}, do not reach the convergence point and demonstrate slower convergence rates relative to I_{E_1}. Although I_{E_1} has not yet attained the convergence point at (1,1), it approaches this point closely. Meanwhile, for the I_E of the MC (without EP), the curves I_{E_1}, I_{E_2}, I_{E_3}, and I_{E_5} are positioned below the I_E curves of the proposed codes (with EP). This result demonstrates that the incorporation of EP facilitates a faster convergence to the desired point.

As the value of ϵ decreases, the elementary EXIT curves are expected to shift upward, indicating improved mutual information exchange and eventual convergence. In this context, the term capacity refers to the capacity of individual polarized subchannels (bit-channels), as determined under the BEC model. In the proposed model with EP, the element I_{E_1} achieves a subchannel capacity of $C = 1$, indicating perfect polarization and optimal bit-channel utilization. The other elements, I_{E_2}, I_{E_3}, and I_{E_5} exhibit subchannel capacities of $C = 0.9853$, $C = 0.9922$, and $C = 0.9634$, respectively, reflecting near-optimal decoding efficiency. In contrast, within the MC structure without EP, the subchannel capacities are notably lower: I_{E_1} reaches $C = 0.9961$, while I_{E_2}, I_{E_3}, and I_{E_5}, yield only $C = 0.8789, C = 0.8086$, and $C = 0.6836$, respectively. These results highlight the enhanced robustness and bit-channel reliability achieved by incorporating EP into the MC. Furthermore, the elementary EXIT curves validate the effectiveness of the proposed bit-channel selection strategy, ensuring that information and frozen bits are optimally placed to improve both the decoding efficiency and the overall system resilience to channel variability.

3-5- Similarity to LDPC Codes

In this paper, we present the construction of the proposed codes, which are similar to the structure of LDPC codes. This similarity may inspire to further coding design of the proposed codes exploiting the decoding scheme commonly adopted in 3GPP standards. Although this work employs SC decoding, belief-propagation (BP) decoding based on the Tanner graph representation could be a potential alternative to further explore performance and complexity trade-offs.

The structure of the proposed codes can be represented in the form of a Tanner graph, a generator matrix **G**, and a parity-check matrix **H** for further potential decoding algorithm, besides the commonly used successive cancellation (SC)-based decoding. The proposed codes utilize simple butterfly XOR operations that support rateless broadband transmissions, chosen for its inherent simplicity and compatibility with efficient hardware implementation.

The Tanner graph representation of **G** and **H** are illustrated in Figure 7 and Figure 8, respectively. The Tanner graph representation of the generator matrix **G** provides a structured framework for analyzing the interactions among variable nodes, check nodes, and edge interleavers. In this representation, variable nodes are depicted as circles and classified

into three categories: (1) information bits, shown as white circles and labeled $\mathbf{u} = [u_1, u_2, u_3, u_5]$; (2) frozen bits, represented by dark gray circles and labeled as f; and (3) EP bits, also represented by dark gray circles and labeled as f. Check nodes, depicted as squares, verify parity constraints, while edge interleavers establish connections between variable nodes and check nodes, ensuring efficient mapping and structural interdependency. Moreover, the nodes labeled as $\mathbf{c} = [c_1, c_2, \cdots, c_{16}]$ represent the codeword generated by the proposed rateless polar coding design.

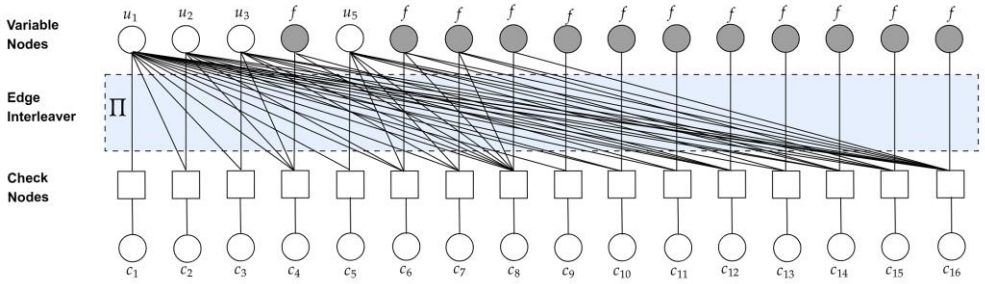

Figure 7. Equivalent Tanner graph of the generator matrix \mathbf{G} for the proposed codes

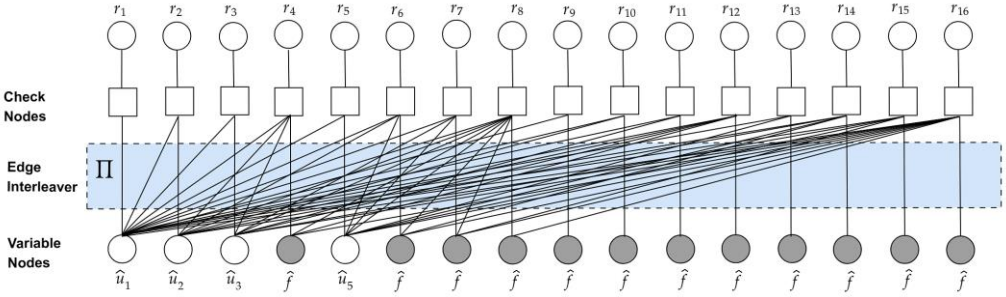

Figure 8. Equivalent Tanner graph of the parity-check matrix \mathbf{H} for the proposed codes

The Tanner graph representation of the **H** matrix for the proposed polar rateless codes provides a visual framework for understanding the decoding process at the receiver. In this structure, the variable nodes labeled as $\mathbf{r} = [r_1, r_2, \cdots, r_{16}]$ represent the received codewords, which serve as inputs for the decoder. The estimated information bits are denoted as $\hat{\mathbf{u}} = [\hat{u}_1, \hat{u}_2, \hat{u}_3, \hat{u}_5]$. Similar to the Tanner graph representation of **G**, the check nodes and edge interleavers of **H** follow the same structural representation.

The generator matrix **G** is designed to support adaptive data transmission and is represented as an 8×16 binary matrix. The matrix rows correspond to variable nodes, while the columns correspond to check nodes. This structure facilitates efficient encoding under varying channel conditions, enabling the dynamic utilization of submatrices of **G** within the EP framework for transmission. The generator matrix **G** is expressed as:

$$\mathbf{G} = \begin{bmatrix} 1&1&1&1&1&1&1&1&1&1&1&1&1&1&1&1 \\ 0&1&0&1&0&1&0&1&0&1&0&1&0&1&0&1 \\ 0&0&1&1&0&0&1&1&0&0&1&1&0&0&1&1 \\ 0&0&0&1&0&0&0&1&0&0&0&1&0&0&0&1 \\ 0&0&0&0&1&1&1&1&0&0&0&0&1&1&1&1 \\ 0&0&0&0&0&1&0&1&0&0&0&0&1&1&1&1 \\ 0&0&0&0&0&0&1&1&0&0&0&0&0&0&1&1 \\ 0&0&0&0&0&0&0&1&0&0&0&0&0&0&0&1 \end{bmatrix} \tag{26}$$

$$\mathbf{H} = \begin{bmatrix} 1&0&0&0&0&0&0&0&0&0&0&0&0&0&0&0 \\ 1&1&0&0&0&0&0&0&0&0&0&0&0&0&0&0 \\ 1&0&1&0&0&0&0&0&0&0&0&0&0&0&0&0 \\ 1&1&1&1&0&0&0&0&0&0&0&0&0&0&0&0 \\ 1&0&0&0&1&0&0&0&0&0&0&0&0&0&0&0 \\ 1&1&0&0&1&1&0&0&0&0&0&0&0&0&0&0 \\ 1&0&1&0&1&0&1&0&0&0&0&0&0&0&0&0 \\ 1&1&1&1&1&1&1&1&0&0&0&0&0&0&0&0 \\ 1&0&0&0&0&0&0&0&1&0&0&0&0&0&0&0 \\ 1&1&0&0&0&0&0&0&0&1&0&0&0&0&0&0 \\ 1&0&1&0&0&0&0&0&0&0&1&0&0&0&0&0 \\ 1&1&1&1&0&0&0&0&0&0&0&1&0&0&0&0 \\ 1&0&0&0&1&0&0&0&0&0&0&0&1&0&0&0 \\ 1&1&0&0&1&1&0&0&0&0&0&0&0&1&0&0 \\ 1&0&1&0&1&0&1&0&0&0&0&0&0&0&1&0 \\ 1&1&1&1&1&1&1&1&0&0&0&0&0&0&0&1 \end{bmatrix} \tag{27}$$

The **H** matrix as presented in (27) is a fundamental component in ensuring error detection and correction for the proposed codes. This 16×16 binary matrix defines the constraints that all valid codewords must satisfy, with each row corresponding to a unique parity-check equation. The matrix structure is designed to capture dependencies among codeword bits, allowing efficient identification of inconsistencies caused by transmission errors. The rows of the matrix correspond to the CNDs, while the columns of the matrix represent VNDs.

4- Performances Evaluation

4-1- BER Performances

The performance of the proposed codes is evaluated through simulations using two error metrics: average BER and average FER. The evaluations are conducted with respect to both signal to noise ratio (SNR) and bit energy-to-noise power spectral density ratio (E_b/N_0) under various channel conditions including AWGN, Rayleigh fading, and fully interleaved channels.

Figure 9 shows the average BER versus average SNR performance of the proposed codes, as described in Figure 2, under the assumption that all transmission links are subject to Rayleigh fading. The average SNR is adopted to characterize overall link quality, as the inherent randomness of Rayleigh fading results in fluctuations of the instantaneous SNR observed at the receiver. Consequently, the average SNR offers a more meaningful metric for evaluating system performance over such fading environments.

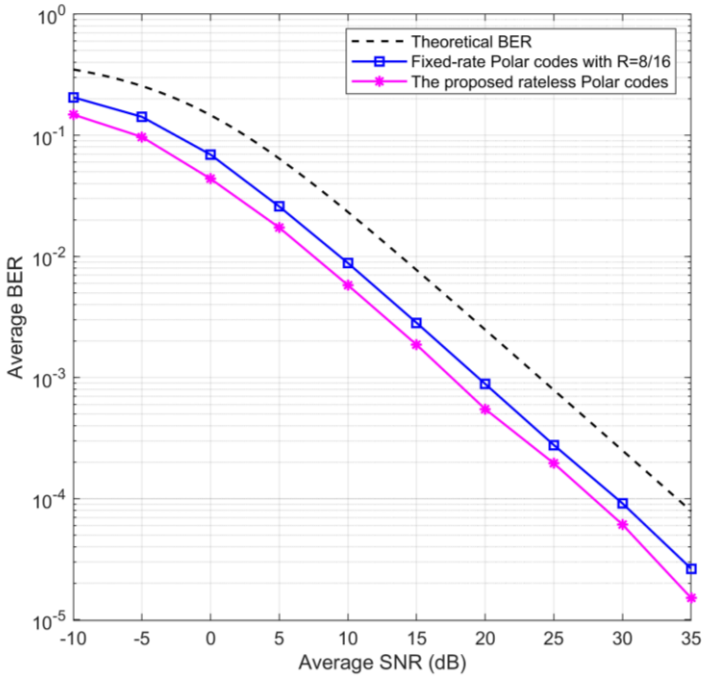

Figure 9. Average BER versus average SNR of the proposed codes for N=16 over Rayleigh fading channel

In the context of rateless channel coding, it is more appropriate to use average SNR rather than average E_b/N_0, since R varies adaptively in response to instantaneous C. For comparison, the figure also presents the theoretical BER curve of uncoded BPSK over Rayleigh fading as a lower-bound reference, along with the BER performance of Arıkan's fixed-rate polar codes as a benchmark for conventional polar codes. This comparison highlights the enhanced adaptability and robustness of the proposed rateless polar scheme in fading channels.

As shown in Figure 9, the proposed codes achieve an overall coding gain of about 7 dB, with 4.5 dB obtained from fixed-rate polar codes and an additional 2.5 dB provided by EP. This result confirms that EP-based XOR operations enhance error resilience while simultaneously strengthening polarization. The EP mechanism facilitates coding rate adjustments to align with C, thereby ensuring performance improvement. Additionally, the proposed design enhances bandwidth efficiency by adaptively adding the EP bits based on prevailing channel conditions. In contrast, fixed-rate polar codes employ a constant number of parity bits irrespective of the channel capacity, resulting in inefficiencies when fewer parity bits could suffice. The average BER performance of the proposed codes demonstrates that the incorporation of butterfly XOR-based EP significantly enhances error correction capability.

Figure 10 presents the average BER performance of the proposed codes over fully interleaved channel conditions at different fixed coding rates: $R = 8/16$ (MC without EP), $R = 8/24$ (MC with 8 EP bits), and $R = 8/32$ (MC with 16 EP bits), as illustrated in Figure 3. Lower coding rates provide improved BER performance due to the increased

redundancy introduced by additional EP bits. The results are plotted against the average E_b/N_0 to enable fair comparisons across different R, as this metric reflects the energy efficiency per information bit. The figure confirms that the proposed scheme enhances reliability as more parity is introduced.

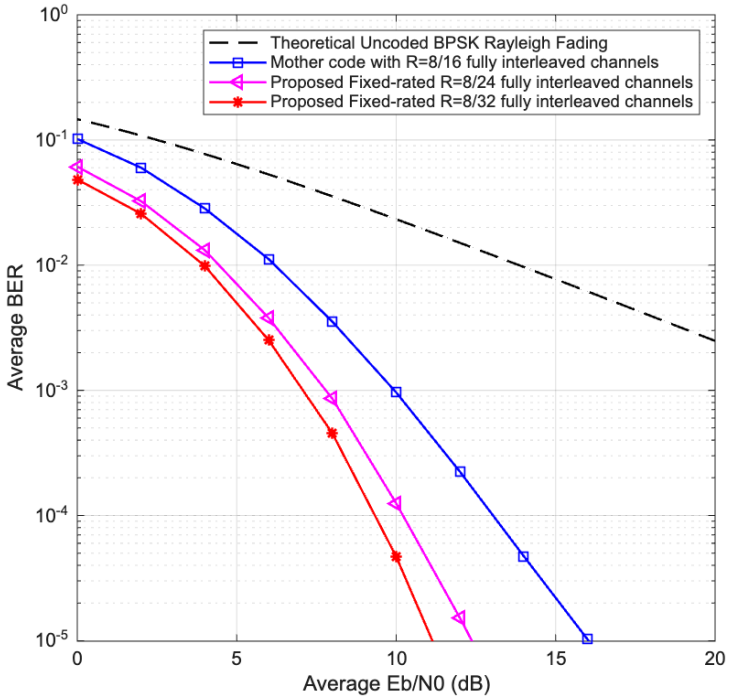

Figure 10. The average BER versus average E_b/N_0 of the proposed codes, as illustrated in Figure 3, with varying R over fully interleaved channels

Figure 11 illustrates the average BER performance of the proposed codes in comparison with repetition codes over three different channel models: Rayleigh fading, fully interleaved, and AWGN, all evaluated at a fixed coding rate of $R = 8/32$. In the AWGN channel, the proposed codes demonstrate superior BER performance at moderate-to-high E_b/N_0 values. Although repetition codes slightly outperform the proposed scheme in the low-SNR region due to their inherent bit-level redundancy, the proposed codes begin to surpass them at approximately $E_b/N_0 = 3\,dB$. This performance improvement results from the enhanced decoding efficiency of the proposed codes under favorable channel conditions.

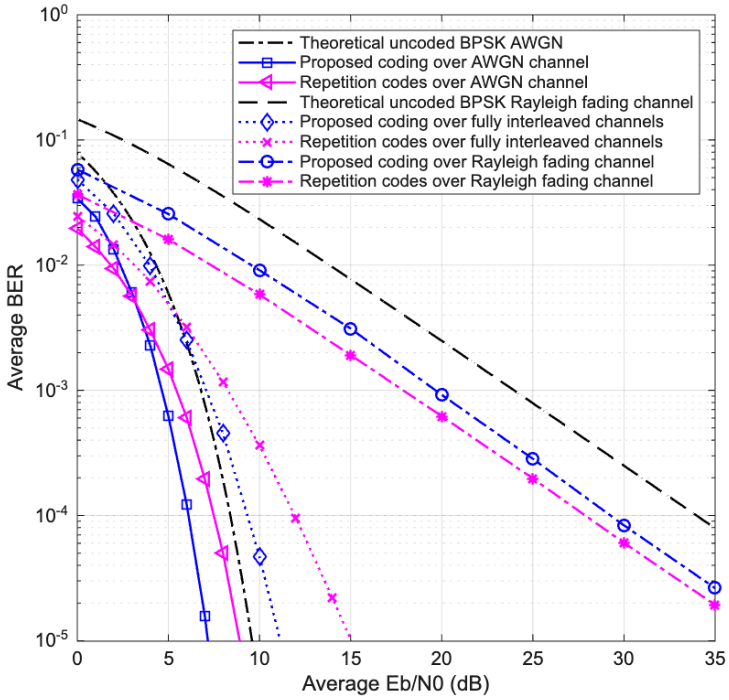

Figure 11. Average BER versus average E_b/N_0 for $R = 8/32$: comparison of the proposed codes and repetition codes over AWGN, fully interleaved, and Rayleigh fading channels

In the fully interleaved channel, which provides ideal diversity by ensuring statistically independent fading across transmitted bits, the proposed scheme significantly outperforms traditional repetition codes. The performance gap becomes more pronounced as E_b/N_0 increases, since the proposed design can effectively exploit channel diversity by distributing information across independent bit-channels. In contrast, the traditional repetition codes are unable to benefit from this property, since the repeating identical bits does not provide additional diversity, leading to degraded performance when some repeated bits experience deep fading. In Rayleigh fading channels, the BER of the proposed scheme is slightly inferior to repetition codes in the low-SNR regime. This is expected due to the severe and random nature of Rayleigh fading, which poses challenges for short block-length decoding. However, as E_b/N_0 increases, the performance of the proposed scheme improves and begins to close the gap with repetition codes.

4-2- FER Performances

The average FER performances of the proposed codes over Rayleigh fading channel are also evaluated, as shown in Figure 12. For benchmarking, the FER curve of fixed-rate polar codes is also presented. Since theoretical FER performance is currently unavailable for rateless transmissions, we use the simulated outage performance of the smallest rate as the baseline for comparison. The simulated outage for $R = 1/2$ provided as the theoretical FER for fixed-rate polar codes confirming that our simulation is valid, since the outage curve matches well to the FER curve of the fixed-rate polar codes. Therefore, the simulated outage for $R = 1/4$, provided as the theoretical FER, is expected to accurately reflect the performance of the proposed codes and support their validity. Simulation results show that the average FER performances of the proposed codes outperform that of the fixed-rate polar codes. For an average FER of approximately 10^{-3}, the SNR required for the proposed codes is about 23 dB, whereas the fixed-rate polar codes require approximately 26.5 dB. For both fixed-rate polar codes and the proposed codes, an anomaly is observed when the average SNR values are negative, as their average FER performance curves deviate from the theoretical outage performance. However, after SNR $\gamma = 0$ dB, the curves adjust accordingly. This phenomenon occurs due to the effects of a short block-length.

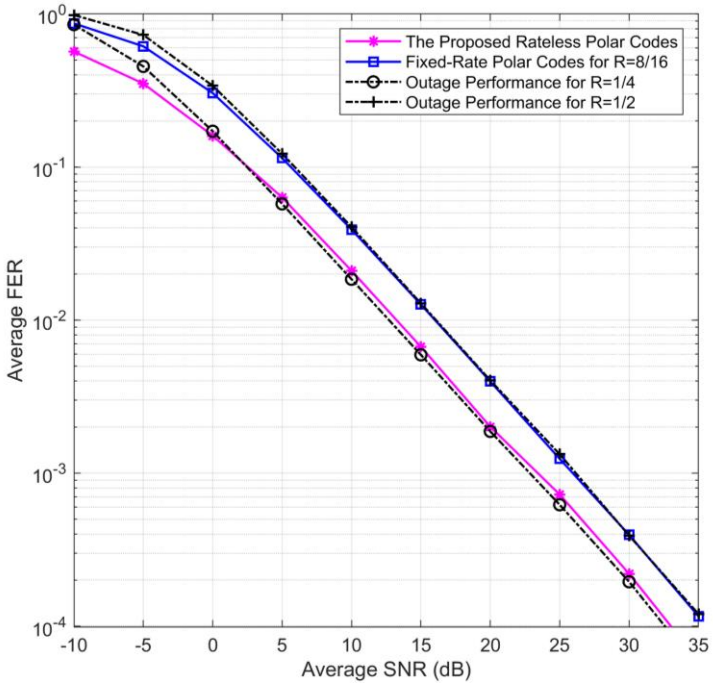

Figure 12. The average FER versus average SNR of the proposed rateless polar codes for N=16 over Rayleigh fading channel

For the fixed-rate polar codes, the simulated outage closely aligns with the FER performance curve, which is also due to the impact of the short block-length. However, as the block-length N increases, the FER curve may shift upwards and surpass the theoretical outage probability curve. This behavior can be attributed to the finite-length effects, where the performance of polar codes is constrained by suboptimal frozen bit allocation and decoding inefficiencies at practical block-lengths. Furthermore, at short block-lengths, the channel polarization process is not fully developed, resulting in a higher proportion of intermediate-quality channels. This complicates the allocation of information and frozen bits, leading to a degradation in performance.

Figure 13 presents the average FER performance of the proposed codes with $R = 8/16$ (MC without EP), $R = 8/24$ (MC with 8 EP bits), and $R = 8/32$ (MC with 16 EP bits) over fully interleaved channels. The results indicate that FER performance improves significantly as the coding rate decreases. The proposed design with $R = 8/32$ achieves the best performance, attributed to its higher redundancy, which enables the decoder to correct a greater number of errors

within a frame. The fully interleaved channel, which offers maximum bit-level diversity, enhances the decoding efficiency of polar codes, particularly when EP bits are incorporated. In contrast, the MC with $R = 8/16$ which lacks additional parity exhibits limited capability in maintaining frame integrity, as reflected by its comparatively higher FER.

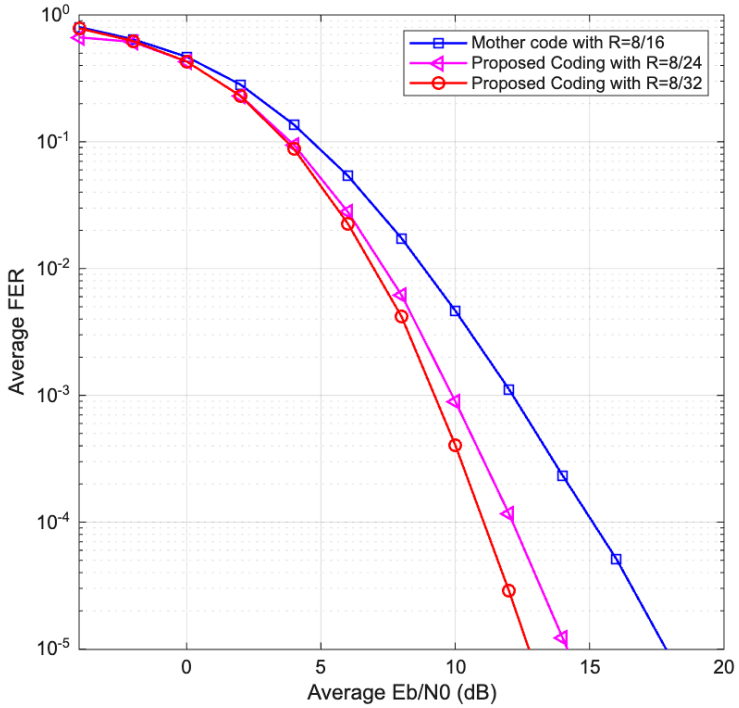

Figure 13. Average FER versus average E_b/N_0 of the proposed rateless polar codes with varying R over fully interleaved channels

Figure 14 illustrates the average FER performance of the proposed codes compared with repetition codes over three different channel models: AWGN, fully interleaved, and Rayleigh fading, all evaluated at a fixed coding rate of $R = 8/32$. Under the AWGN channel, the proposed codes consistently achieve lower FER across the entire E_b/N_0 range. This indicates enhanced robustness in preserving frame integrity, particularly at moderate-to-high E_b/N_0 levels. Although repetition codes provide slightly better BER at low SNR, their lack of structured decoding results in a higher probability of total frame failure when multiple bit errors occur. In contrast, the proposed codes are capable of localizing and correcting scattered errors, significantly improving overall frame reliability.

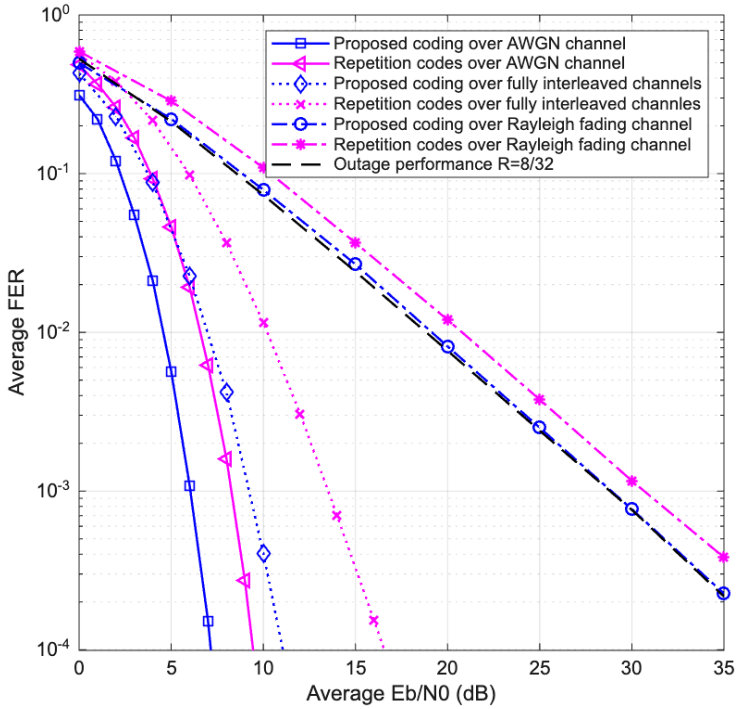

Figure 14. Average FER versus E_b/N_0 for $R = 8/32$: comparison of the proposed rateless polar codes and repetition codes over AWGN, fully interleaved, and Rayleigh fading channels

In the fully interleaved channel, which simulates ideal diversity where each bit experiences independent fading, the proposed codes outperform repetition codes by a substantial margin. This performance gain becomes more pronounced at higher E_b/N_0, reflecting the ability of polar codes to exploit channel diversity through bit-channel polarization. The EP structure of the proposed design further enhances its capability to recover from deep fades, whereas repetition codes are more susceptible to frame loss if any of the repeated bits are corrupted. Under Rayleigh fading conditions, the proposed scheme also demonstrates superior FER performance, closely approaching the theoretical outage probability at high E_b/N_0. While BER may be slightly degraded due to the unpredictable nature of Rayleigh fading and short block-length constraints, the proposed decoder effectively mitigates these challenges by preserving overall frame correctness. This confirms the proposed scheme's robustness in fading-dominated environments.

The simulation results across three channel models, namely AWGN, fully interleaved, and Rayleigh fading, demonstrate that the proposed codes consistently achieve superior performance in terms of FER, while also maintaining competitive BER performance at moderate-to-high E_b/N_0 levels. In low-SNR regions, repetition codes may exhibit slightly better BER due to their inherent bit-level redundancy. However, as E_b/N_0 increases, the decoding efficiency and polarization structure of the proposed scheme result in significant BER improvements. More notably, the proposed codes maintain lower FER across all channel conditions, reflecting their strong capability in preserving overall frame integrity despite the presence of scattered bit errors or channel fading. These findings confirm that the proposed codes offer a reliable and efficient solution for broadband transmission.

In this paper, the baselines are limited to conventional repetition codes and fixed-rate polar codes. This selection is intentional, since the proposed exploits the principle of repetition, where simple XOR operations do not only support polarization but also strengthen the rateless property. By contrast, LT/Raptor-like rateless schemes rely on distinct graph-based constructions and exhibit different complexity trade-offs; therefore, a rigorously tuned short block-length comparison with such schemes falls beyond the scope of this work.

4-3- Computational Complexity of The Proposed Codes

In this paper, we analyze the computational complexity of the proposed codes by extending the complexity framework of Arıkan's polar codes. Including the EP bits results in a linear increase in the number of butterfly units. Adding a single EP bit requires a single additional butterfly unit. Similarly, adding two EP bits requires two additional butterfly units. Please note that the addition of a single butterfly unit corresponds to an additional XOR operation.

Based on the complexity of polar codes by Arıkan, the overall complexity can be approximated as $2X$, where X denotes the number of XOR operations. Since the addition of e EPs corresponds to e XORs, the total computational complexity of the proposed codes can be approximated as the sum of the computational complexity of the MC and that of the EP. For a mother code with $R = 1/2$ the computational complexity is expressed as:

$$R = \frac{\frac{1}{2}N}{N} \Rightarrow C = N\,log\,N. \tag{28}$$

Therefore, the computational complexities of the proposed rateless polar codes based on Equation 28 are expressed as:

$$R = \frac{\frac{1}{2}N}{N+1} \Rightarrow C = N\,log\,N + 2, \tag{29}$$

$$R = \frac{\frac{1}{2}N}{N+2} \Rightarrow C = N\,log\,N + 4, \tag{30}$$

and for general e EPs as

$$R = \frac{\frac{1}{2}N}{N+e} \Rightarrow C = N\,log\,N + 2e, \tag{31}$$

Since e cannot be very large*, we need to understand relationship between e and N, which can be derived as

$$e = \left(\frac{1}{2R} - 1\right)N. \tag{32}$$

The limit value of e in Equation 32 is infinite if $R \to 0$. For practical purposes, the coding rate R must not approach zero. Since the total computational complexity is given by the expression in Equation 31, an excessive number of EP bits would result in significantly increased complexity, rendering real-time implementation infeasible. Additionally, an extremely low coding rate implies that the transmitted codeword consists predominantly of parity bits rather than information bits, which contradicts the fundamental objective of rateless coding with efficient adaptation to varying channel conditions. Therefore, a lower bound on R is necessary to maintain a balance between redundancy, computational complexity, and overall transmission efficiency.

* It is under constraint of latency.

Table 2 summarizes the computational complexity of the proposed codes as a function of N and e. For the baseline computational complexity, we use the computational complexity of polar codes with $e = 0$ (MC) having $R = {}^{1}/_{2}\, N/N$ of which the complexity is $N\ log\ N$. As additional EP bits are incorporated, the coding rate decreases progressively from $R = {}^{1}/_{2}\, N/(N+1)$ to $R = {}^{1}/_{2}\, N/(N+e)$ for addition of e EP bits, while the computational complexity increases by $2e$ from the baseline computational complexity as shown in Table 2. It indicates that while the dominant terms $N\ log\ N$ governs the scaling of computational complexity with increasing N, the inclusion of EP bits introduces a fixed overhead that grows linearly with e. Consequently, although e can enhance performance metrics such as rate adaptability and error correction capability, they also lead to a predictable increase in computational complexity. However, this trade-off becomes less significant as the block-length increases.

Table 2. Coding rate and complexity for different numbers of EP

Number of EPs	Coding Rate (R)	Complexity
0	${}^{1}/_{2}\, N/N$	$N \log N$
1	${}^{1}/_{2}\, N/(N+1)$	$N \log N + 2$
2	${}^{1}/_{2}\, N/(N+2)$	$N \log N + 4$
3	${}^{1}/_{2}\, N/(N+3)$	$N \log N + 6$
4	${}^{1}/_{2}\, N/(N+4)$	$N \log N + 8$
5	${}^{1}/_{2}\, N/(N+5)$	$N \log N + 10$
6	${}^{1}/_{2}\, N/(N+6)$	$N \log N + 12$
7	${}^{1}/_{2}\, N/(N+7)$	$N \log N + 14$
8	${}^{1}/_{2}\, N/(N+8)$	$N \log N + 15$
⋮	⋮	⋮
e	${}^{1}/_{2}\, N/(N+e)$	$N \log N + 2e$

As the proposed EP mechanism requires only simple XOR operations appended to the standard polar transform, the resulting increase in computational complexity is negligible. Accordingly, the additional hardware overhead is minimal and does not significantly affect power consumption. Moreover, given that MTC and IoT devices operate with short block-length and low-latency transmissions, the added EP operations are expected to remain energy-efficient in practice. A detailed hardware power analysis is considered beyond the scope of this work.

5- Conclusion

We have proposed a new design of rateless polar codes using EP for broadband transmissions. The proposed codes employed butterfly XOR operations to generate the EP, incorporating all bits of the MC to enhance error correction performance by exploiting channel diversity. The proposed structure reflected the principle of repetition, where simple XOR operations do not only facilitate polarization but also reinforce the rateless property. Furthermore, the proposed structure preserved the standard polar transform and decoding graph, and therefore can be scaled like Arikan's original polar codes. The proposed codes were evaluated through simulations over Rayleigh fading, fully interleaved, and additive white Gaussian noise (AWGN) channels. Simulation results demonstrated that the proposed codes achieved significant performance improvements, particularly over fully interleaved channels, indicating that the XOR-based EP structure exploits channel diversity, which is the characteristic of broadband channels. In the case of a coding rate $R = 4/16$, the proposed codes outperformed conventional fixed-rate polar codes in terms of BER and FER. The observed total coding gain was approximately 7 dB, comprising a 4.5 dB gain from the fixed-rate polar codes and an additional 2.5 dB gain attributed to the EP mechanism. This performance enhancement indicates that the proposed structure can effectively adapt to varying channel conditions by maintaining $R \leq C$. This improvement is paid by the introduction of only a minor increase in computational complexity. The proposed structure is well-suited for dynamic channel environments and demonstrates high effectiveness in broadband scenarios, where channel diversity can be fully leveraged.

6- Declarations

6-1- Author Contributions

Conceptualization, Y.S.R., I., K.A., and M.S.A.; methodology, Y.S.R. and K.A.; software, Y.S.R.; validation, Y.S.R., I., K.A., and M.S.A.; formal analysis, Y.S.R. and K.A.; investigation, I. and M.S.A.; resources, Y.S.R., I., K.A., and M.S.A.; data curation, Y.S.R.; writing—original draft preparation, Y.S.R.; writing—review and editing, Y.S.R., I., K.A., and M.S.A.; visualization, Y.S.R.; supervision, I., K.A., and M.S.A.; project administration, Y.S.R.; funding acquisition, Y.S.R. All authors have read and agreed to the published version of the manuscript.

6-2- Data Availability Statement

The data presented in this study are available on request from the corresponding author.

6-3- Funding

The authors received partial financial support for the publication of this article. The article processing charge (APC) was partially covered by the authors affiliated institution. No external funding was received for the research and authorship.

6-4- Institutional Review Board Statement

Not applicable.

6-5- Informed Consent Statement

Not applicable.

6-6- Conflicts of Interest

The authors declare that there is no conflict of interest regarding the publication of this manuscript. In addition, the ethical issues, including plagiarism, informed consent, misconduct, data fabrication and/or falsification, double publication and/or submission, and redundancies have been completely observed by the authors.

7- References

[1] Miao, S., Kestel, C., Johannsen, L., Geiselhart, M., Schmalen, L., Balatsoukas-Stimming, A., Liva, G., Wehn, N., & Brink, S. Ten. (2024). Trends in Channel Coding for 6G. Proceedings of the IEEE, 112(7), 653–675. doi:10.1109/JPROC.2024.3416050.

[2] Yang, H., Liang, E., Pan, M., & Wesel, R. D. (2022). CRC-Aided List Decoding of Convolutional Codes in the Short Blocklength Regime. IEEE Transactions on Information Theory, 68(6), 3744–3766. doi:10.1109/TIT.2022.3150717.

[3] Sui, W., Towell, B., Asmani, A., Yang, H., Grissett, H., & Wesel, R. D. (2024). CRC-Aided High-Rate Convolutional Codes with Short Blocklengths for List Decoding. IEEE Transactions on Communications, 72(1), 63–74. doi:10.1109/TCOMM.2023.3324370.

[4] Ranganathan, S. V. S., Divsalar, D., & Wesel, R. D. (2019). Quasi-Cyclic Protograph-Based Raptor-Like LDPC Codes for Short Block-Lengths. IEEE Transactions on Information Theory, 65(6), 3758–3777. doi:10.1109/TIT.2019.2895322.

[5] Arikan, E. (2009). Channel polarization: A method for constructing capacity-achieving codes for symmetric binary-input memoryless channels. IEEE Transactions on Information Theory, 55(7), 3051–3073. doi:10.1109/TIT.2009.2021379.

[6] Piao, J., Niu, K., Dai, J., & Dong, C. (2020). Approaching the Normal Approximation of the Finite Blocklength Capacity within 0.025 dB by Short Polar Codes. IEEE Wireless Communications Letters, 9(7), 1089–1092. doi:10.1109/LWC.2020.2981432.

[7] Choi, G., & Lee, N. (2024). Deep Polar Codes. IEEE Transactions on Communications, 72(7), 3842–3855. doi:10.1109/TCOMM.2024.3374355.

[8] Nurbani, C. A., Anwar, K., & Cahyadi, W. A. (2021). Hybrid Multikernel-Constructed Polar Codes for Short Blocklength Transmissions. 2021 International Wireless Communications and Mobile Computing (IWCMC), 724–728. doi:10.1109/iwcmc51323.2021.9498898.

[9] Gamage, H., Ranasinghe, V., Rajatheva, N., & Latva-aho, M. (2020). Low Latency Decoder for Short Blocklength Polar Codes. 2020 European Conference on Networks and Communications (EuCNC), 305–310. doi:10.1109/eucnc48522.2020.9200964.

[10] Wan, H., & Nosratinia, A. (2023). Short-Block Length Polar-Coded Modulation for the Relay Channel. IEEE Transactions on Communications, 71(1), 26–39. doi:10.1109/TCOMM.2022.3225546.

[11] Luby, M. (2002). LT codes. The 43rd Annual IEEE Symposium on Foundations of Computer Science. Proceedings. doi:10.1109/SFCS.2002.1181950.

[12] Tian, S., Li, Y., Shirvanimoghaddam, M., & Vucetic, B. (2013). A physical-layer rateless code for wireless channels. IEEE Transactions on Communications, 61(6), 2117–2127. doi:10.1109/TCOMM.2013.042313.120159.

[13] Anggraeni, C. D., & Anwar, K. (2021). Design of Rateless Polar Accumulate Tornado Codes Using EXIT Chart for UAV Communications. 2021 IEEE Symposium on Future Telecommunication Technologies (SOFTT), 63–68. doi:10.1109/SOFTT54252.2021.9673142.

[14] Sobiroh, I. F. E., Anwar, K., & Mukhtar, H. (2020). Rateless Raptor Codes for Reliable Wireless Capsule Endoscopy (WCE). 2020 27th International Conference on Telecommunications (ICT), 1–5. doi:10.1109/ict49546.2020.9239424.

[15] Borujeny, R. R., & Ardakani, M. (2016). A new class of rateless codes based on reed-solomon codes. IEEE Transactions on Communications, 64(1), 49–58. doi:10.1109/TCOMM.2015.2502952.

[16] Liang, H., Liu, A., Zhang, Y., Cheng, F., & Yi, X. (2018). A Throughput-Efficient Rateless Scheme of Polar Codes. 018 10th International Conference on Wireless Communications and Signal Processing (WCSP), 1–7. doi:10.1109/WCSP.2018.8555651.

[17] Schnelling, C., Rothe, M., Mathar, R., & Schmeink, A. (2018). Rateless Codes Based on Punctured Polar Codes. 2018 15th International Symposium on Wireless Communication Systems (ISWCS), 1–5. doi:10.1109/ISWCS.2018.8491237.

[18] Liang, H., Liu, A., Cheng, F., & Liang, X. (2019). Rateless Polar-Spinal Coding Scheme with Enhanced Information Unequal Error Protection. IEEE Access, 7, 145996–146004. doi:10.1109/ACCESS.2019.2946167.

[19] Feng, B., Zhang, Q., & Jiao, J. (2017). An Efficient Rateless Scheme Based on the Extendibility of Systematic Polar Codes. IEEE Access, 5, 23223–23232. doi:10.1109/ACCESS.2017.2762363.

[20] Li, B., Tse, D., Chen, K., & Shen, H. (2016). Capacity-achieving rateless polar codes. 2016 IEEE International Symposium on Information Theory (ISIT), 46–50. doi:10.1109/ISIT.2016.7541258.

[21] Liang, H., Liu, A., Gong, C., & Liu, X. (2020). Rateless Coding Schemes Using Polar Codes: Truly "No" Rates? IEEE Access, 8, 2428–2440. doi:10.1109/ACCESS.2019.2962056.

[22] Liu, S., Hong, Y., & Viterbo, E. (2017). Polar Codes for Block Fading Channels. 2017 IEEE Wireless Communications and Networking Conference Workshops (WCNCW), 1–6. doi:10.1109/WCNCW.2017.7919041.

[23] Niu, K., & Li, Y. (2021). Polar Coded Diversity on Block Fading Channels via Polar Spectrum. IEEE Transactions on Signal Processing, 69, 4007–4022. doi:10.1109/TSP.2021.3094652.

[24] Brink, S. Ten. (2001). Convergence behavior of iteratively decoded parallel concatenated codes. IEEE Transactions on Communications, 49(10), 1727–1737. doi:10.1109/26.957394.

[25] Gallager, R. (1962). Low-density parity-check codes. IEEE Transactions on Information Theory, 8(1), 21–28. doi:10.1109/tit.1962.1057683.

[26] Ten Brink, S., Kramer, G., & Ashikhmin, A. (2004). Design of low-density parity-check codes for modulation and detection. IEEE Transactions on Communications, 52(4), 670–678. doi:10.1109/TCOMM.2004.826370.

[27] Mufassa, F. H., & Anwar, K. (2019). Extrinsic Information Transfer (EXIT) Analysis for Short Polar Codes. 3rd Symposium on Future Telecommunication Technologies, SOFTT 2019, 1-6. doi:10.1109/SOFTT48120.2019.9068617.